COBEM UBERLÂNDIA 2019

ABCM Associação Brasileira de Engenharia e Ciências Mecânicas

25th ABCM International Congress of Mechanical Engineering
October 20-25, 2019, Uberlândia, MG, Brazil

PARTICLE DAMPING IN ROTATING CANTILEVER BEAMS

Leonardo Masson Oliveira
Rodrigo Nicoletti
Universidade de São Paulo, Escola de Engenharia de São Carlos, Departamento de Engenharia Mecânica, Trabalhador São Carlense 400, 13566-590 São Carlos, SP, Brazil
leonardo.masson.oliveira@usp.br, rnicolet@sc.usp.br

Abstract. *Rotating blades can present catastrophic failure due to excessive blade vibration. One way of adding damping to a rotating blade, thus reducing vibration responses, is to adopt the so called particle dampers. Particle dampers are passive attenuating mechanisms of vibration, where small to medium sized particles are introduced into the structure to dissipate energy. In this work, the idea is to drill holes in the longitudinal direction of the turbine blades and fill them with particles to increase structure damping and reduce blade vibration responses. We adopt bigger particles (steel spheres of 5 mm diameter) and the spheres are free to vibrate in the structure. Therefore, the particles will present shock inside the blade as an energy dissipation mechanism. In addition, we include the effect of rotation to the blade, which will impose to the spheres an increasing normal force due to centrifugal effects. The results show the effectiveness of reducing resonance peaks in the response function of the structure.*

Keywords: *friction, blades, structure dynamics, vibration attenuation*

1. INTRODUCTION

Rotating systems can be found in the whole production chain, from raw material sourcing (prospection, extraction, energy generation), through manufacturing processes in industry, up to finished products for customers. Considering the broad application of rotating systems, one can infer its importance in the productive system and the economic consequences of eventualities, malfunctioning or failure. For this reason, the design of large rotating systems, such as gas turbines, steam turbines, and compressors, is subjected to requirements of high efficiency, low fuel consumption, low weight (aeronautic applications) and, most importantly, high reliability and life of its components.

Despite the strict requirements and norms rotating system design is subjected to, components can eventually fail under unpredicted, or off-the-norm, operating conditions. As a result, non programmed operation stops are necessary for maintenance, resulting in serious economic losses, or even catastrophic losses. Specifically in the case of rotating blades, numerous examples of catastrophic failure can be found in literature (Yu and Xu, 2009; Kubiak *et al.*, 2009; Lourenço *et al.*, 2008), where they started by blade root cracking, leading to a fatigue process, finally resulting in blade loss and overall damage (Fig. 1). In most of the cases, such failure process was caused by excessive blade vibration, which can occur due to fluid induced vibration (flutter), non-symmetric assembling (localized modes), low aspect ratio blades, or forced response from environmental and operating conditions. If blade vibration could be somehow controlled during operation, or at least attenuated, maybe some of these failure cases could have been prevented.

(a) 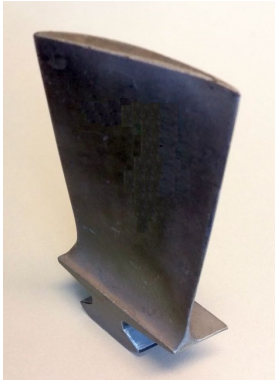 (b) 

Figure 1. Gas turbine blades: (a) low pressure stage blade (slender blade), (b) catastrophic failure (Kubiak *et al.*, 2009).

Slender gas turbine blades are essentially rotating cantilever beams. One way of adding damping to a cantilever beam, thus reducing vibration responses, is by using the so called *particle dampers* (Lu *et al.*, 2018). Particle dampers are passive attenuating mechanisms of vibration, where small to medium sized particles are introduced in the structure to dissipate energy. Most of the examples in literature of particle dampers refer to particles that are free to move, shock and rub inside the structure. For example, Koch *et al.* (2017) present experimental results of a honeycomb structure with granular material, applied to the oil pan bottom of a combustion engine. The results show that higher dampening effects are observed when the material is located in the areas of higher vibration amplitudes. In addition, damping increases with the increase of the mass of granular material used. This later conclusion was theoretically predicted by Cui *et al.* (2011).

In the present work, the idea is to drill holes in the longitudinal direction of the turbine blades and fill them with particles to increase structure damping and reduce blade vibration responses. Something in this direction was studied by (Xu *et al.*, 2004) (experimentally) and (Xu *et al.*, 2005) (numerically) on beams and plates, using small tungsten carbide particles. The results showed a strong rate of dissipation within a broadband range of frequencies. The difference here is that we adopt bigger particles (steel spheres of 5 mm diameter) in a rotating structure. Therefore, the particles will present no shock as an energy dissipation mechanism. In addition, we will include the effect of rotation, which will impose to the spheres an increasing normal force due to centrifugal effects.

2. MATHEMATICAL MODELING OF THE ROTATING BEAM WITH PARTICLES

The geometry of the blade will be simplified to that of a cantilever beam, whose properties are listed in Table 1. Four different beams are studied for comparison: beam without particles, beam with a hole of 50 mm length filled with 10 spheres, beam with a hole of 100 mm length filled with 20 spheres, and beam with a hole of 200 mm length filled with 40 spheres. The holes are drilled from the constrained end of the beam towards its center (Fig. 2). The material of the beam is aluminum and the material of the spheres is steel.

Table 1. Properties of the cantilever beam and particles in study.

beam Young modulus	69 MPa	length of the holes	50, 100, 200 mm
beam density	2,700 kg.m^{-3}	diameter of the holes	5.2 mm
beam length	270 mm	diameter of the spheres	5.0 mm
beam width	38 mm	number of spheres per hole	10, 20, 40
beam height	12 mm		

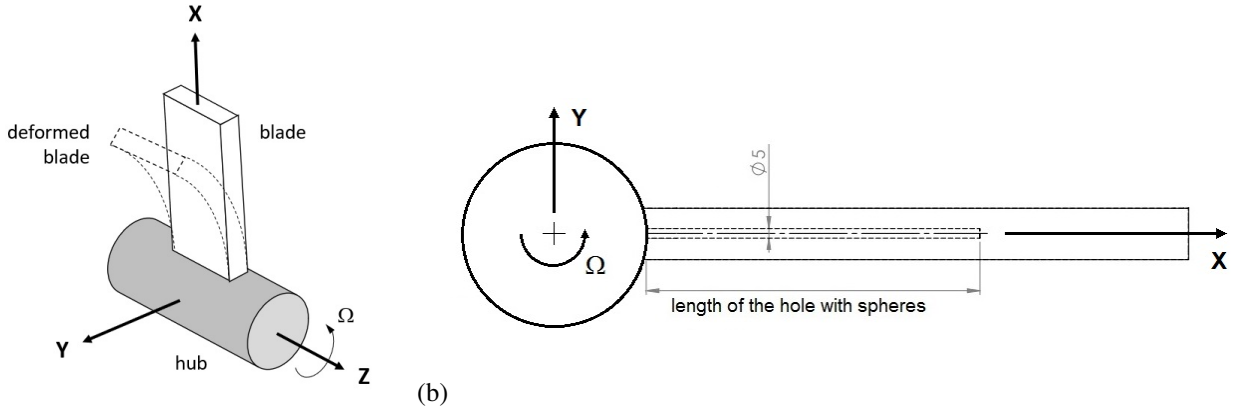

Figure 2. Rotating cantilever beam: (a) rotating reference system of the mathematical model, (b) position of the hole in the beam.

The beam is modeled via finite elements (Euler-Bernoulli beam theory), considering the presence of the hole in the cross section area of the beam. The adopted finite beam element has four degrees-of-freedom in each node, according to the reference system depicted in Fig. 2: axial displacement u in X direction, the derivative $\theta_u = du/dx$, the tangential (out-of-plane) displacement v in Y direction, and the derivative $\theta_v = dv/dx$. The resultant equations of motion of the beam are:

$$\mathbf{M}\,\ddot{\mathbf{q}} + (\mathbf{D} + \mathbf{G})\,\dot{\mathbf{q}} + (\mathbf{K} + \mathbf{K}_\Omega)\,\mathbf{q} = \mathbf{f} \tag{1}$$

where $\mathbf{M}$ is the inertia matrix, $\mathbf{D}$ is the structural damping matrix, $\mathbf{G}$ is the gyroscopic matrix, $\mathbf{K}$ is the elastic stiffness matrix, $\mathbf{K}_\Omega$ is the centrifugal stiffness matrix, $\mathbf{f}$ is the force vector, and $\mathbf{q}$ is the vector of degrees-of-freedom of the model.

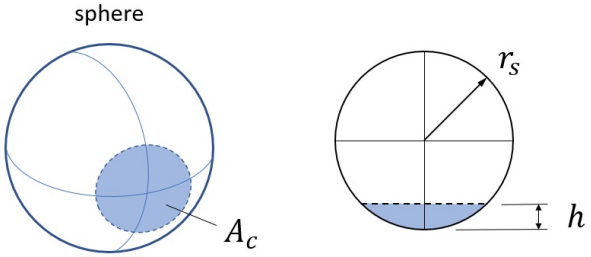

Figure 3. Contact area between the sphere and the wall of the beam hole.

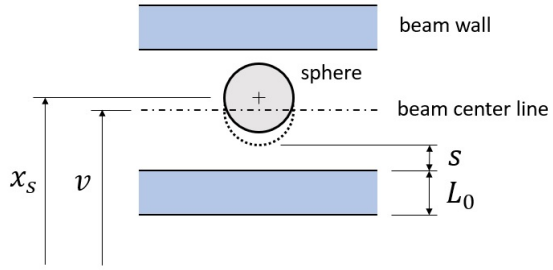

Figure 4. Displacement of the sphere inside the hole of the beam.

The finite element matrices are listed in the Appendix, and are based on the model presented in Nicoletti and Liebich (2018). We adopted damping ratios of 0.01 and 0.001 for the first and second mode shapes of the beam, respectively.

The spheres are modeled as lumped masses (steel spheres of 0,5 g), subjected to a contact force F_c between the sphere and the surface of the hole in the beam. Therefore, the equation of motion of the i-th sphere is:

$$m_{si}\ddot{x}_{si} = F_{ci} \tag{2}$$

where m_{si} is the mass of the i-th sphere, x_{si} is the displacement of the i-th sphere, and F_{ci} is the contact force between the i-th sphere and the beam.

The contact force is obtained from the deformation of the surface of the beam caused by the the sphere in contact, which is considered rigid. Hence:

$$F_{ci} = E\,A_{ci}\,\varepsilon = E\,A_{ci}\frac{h}{L_0} \tag{3}$$

where E is the Young modulus of the beam, A_{ci} is the contact area between the i-th sphere and the surface of the beam, ε is the strain of the beam, h is the deformation of the beam, and L_0 is the thickness of the wall (Figs. 3 and 4). Considering that:

$$A_{ci} = 2\pi r_s h \tag{4}$$

where r_s is the radius of the sphere (Fig. 3), then:

$$F_{ci} = \begin{cases} \dfrac{2\pi r_s E h^2}{L_0}, & \text{if} \quad v_i - x_{si} \geq s \\ 0, & \text{if} \quad -s < (v_i - x_{si}) < s \\ -\dfrac{2\pi r_s E h^2}{L_0}, & \text{if} \quad v_i - x_{si} \leq -s \end{cases} \tag{5}$$

where $h = v_i - x_{si}$, v_i is the out-of-plane displacement of the beam in the i-th node, x_{si} is the displacement of the i-th spehre, s is the nominal gap between the sphere and the hole in the beam ($s = r_h - r_s$), and r_h is the hole radius (see Fig. 4). Equation (5) estates that the contact force acting on the sphere is positive if the displacement of the beam is greater than the displacemnt of the sphere plus the gap; the contact force is negative if the displacement of the beam is smaller than the displacement of the sphere minus the gap; and the contact force is null otherwise (when the sphere is in the hole without any contact to the walls). Such contact force is applied to the respective node of the finite element model of the beam, with counter sign as a reaction force.

3. NUMERICAL RESULTS

The system is numerically simulated for different rotating speeds. The first two natural frequencies of the beam under null rotation are 135 Hz and 851 Hz. As the beam rotates, there is a shifting of the natural frequencies towards higher values (Fig. 5a). This is caused by the centrifugal forces acting on the beam, thus resulting in a stiffening effect. As we can see, the model is able to capture such effect, which is higher on the first natural frequency in comparison to effect on the second natural frequency. By calculating the frequency response function (FRF) of the beam, this stiffening effect becomes clearer, as the resonance peaks move towards higher frequencies (Fig. 5b)

To compare the behavior of the beam with the spheres, we calculate the resultant frequency response of the beam. For that, the model is reduced by modal decoupling (Thomson and Dahleh, 1998), considering the first two natural frequencies of the beam. A chirp signal force is applied to the tip of the beam in flapwise direction and the response of the beam is

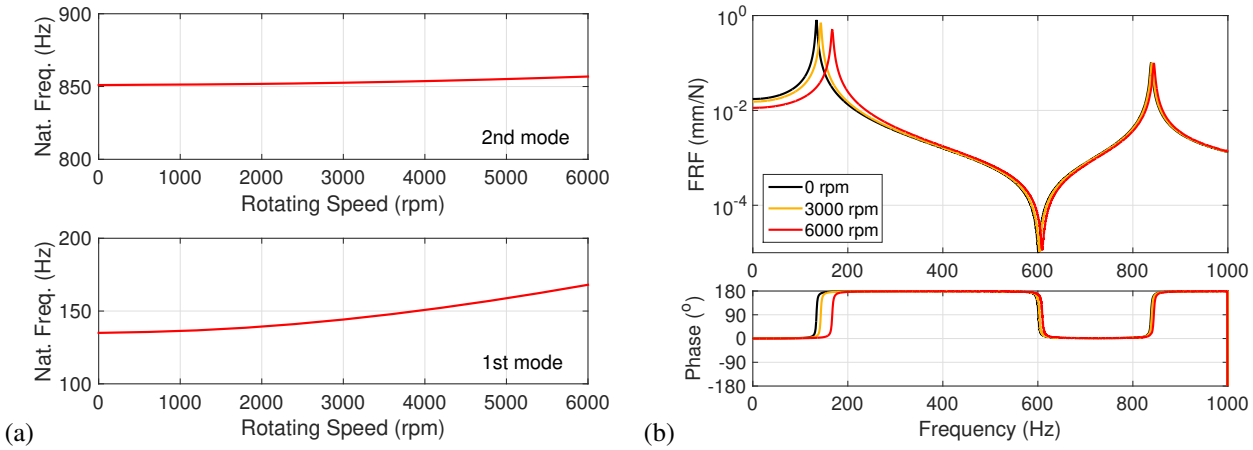

Figure 5. The stiffening effect due to rotation: (a) variation of the natural frequencies, (b) frequency response functions at the tip of the rotating beam.

calculated by numerical integration of the equations of motion (Eqs.(1) and (2)). We adopted the low order method for nonstiff differential equations `ode23` in MatLab to integrate the non-linear equations of motion.

Figure 6 presents the obtained results for the four different beams in study (no sphere, 10 spheres, 20 spheres, and 40 spheres) for the rotating speed of 3000 rpm. As we can see in Fig. 6b, the presence of 10 spheres in the beam reduces its second resonance peak, and the beam presents a scattered vibration. Such scattered vibration comes from the interation between the beam and the bouncing spheres inside the beam. By increasing the number of spheres to 20 (Fig. 6c), we see that the first resonance peak is also affected, and scattered vibration appears. By comparing these results to those of obtained with 10 spheres (Fig. 6b), we note that the scattered vibration at the second resonance is also reduced with 20 spheres. By further increasing the number of spheres to 40 (Fig. 6d), we see no resonances in the system. In this last case, the amount of spheres is big enough to dampen the response of the beam in its two first resonances.

It is important to note that, such behavior is strongly nonlinear. Therefore, the results obtained in Fig. 6 depend on the level of excitation applied to the beam and on the size of the gap between the spheres and the beam hole. In this case, we applied a chirp signal with amplitude of 10 N, and the gap was 0.1 mm. For example, by increasing the gap to 0.3 mm and 0.5 mm for the 10 sphere case (Fig. 7), we see a decrease of the dampening effect on the second resonance of the system. In fact, if the gap is big enough, the vibration response of the beam will be smaller than the gap, and there will be no significative contact between the spheres and the beam. As a consequence, the damper system does not work and the beam presents the behavior of a beam without spheres, which is the case of a 0.5 mm gap (Fig. 7b). Larger excitaton forces will lead to larger vibrating amplitudes of the beam, thus increasing the chance of contact between the spheres and the beam.

This relationship between beam vibration amplitude and the gap between the spheres and the beam explains why the second resonance is affected by the particle damper with 10 spheres (50 mm hole length) and the frist resonance not. If we look at the resonance amplitudes along the beam in Fig. 6a, we see that the second mode shape of the beam presents higher amplitudes in the range of 0 to 50 mm of the beam than the first mode shape. For this reason, the damper with 10 spheres will only work in the second resonance, because in the first resonance, the vibration amplitude of the beam between 0 and 50 mm is not as big as that of the gap. When we adopt longer dampers (100 mm and 200 mm), we reach regions of the beam with higher amplitudes, and we start having contact between the spheres and the beam in the first resonance of the system.

If we increase the rotating speed of the system, we note no significative difference in the results. Although the centrifugal forces are higher at higher rotating speeds, we have to consider that the structure is also stiffer due to the centrifugal stiffening effect as the beam rotates. It seems that one effect compensates the other in this case.

4. CONCLUSION

This work focuses on the application of particle damping to rotating cantilever beams (with possible application to rotating blades). The main conclusions of this work are:

- the presence of particles (spheres) inside the beam does result in a significant attenuation of its resonance peaks. As the damper works, resonance is substituted by scattered vibration due to the interaction between the spheres and the beam;

- such attenuation depends on the level of vibration of the beam and on the gap between the spheres and the beam.

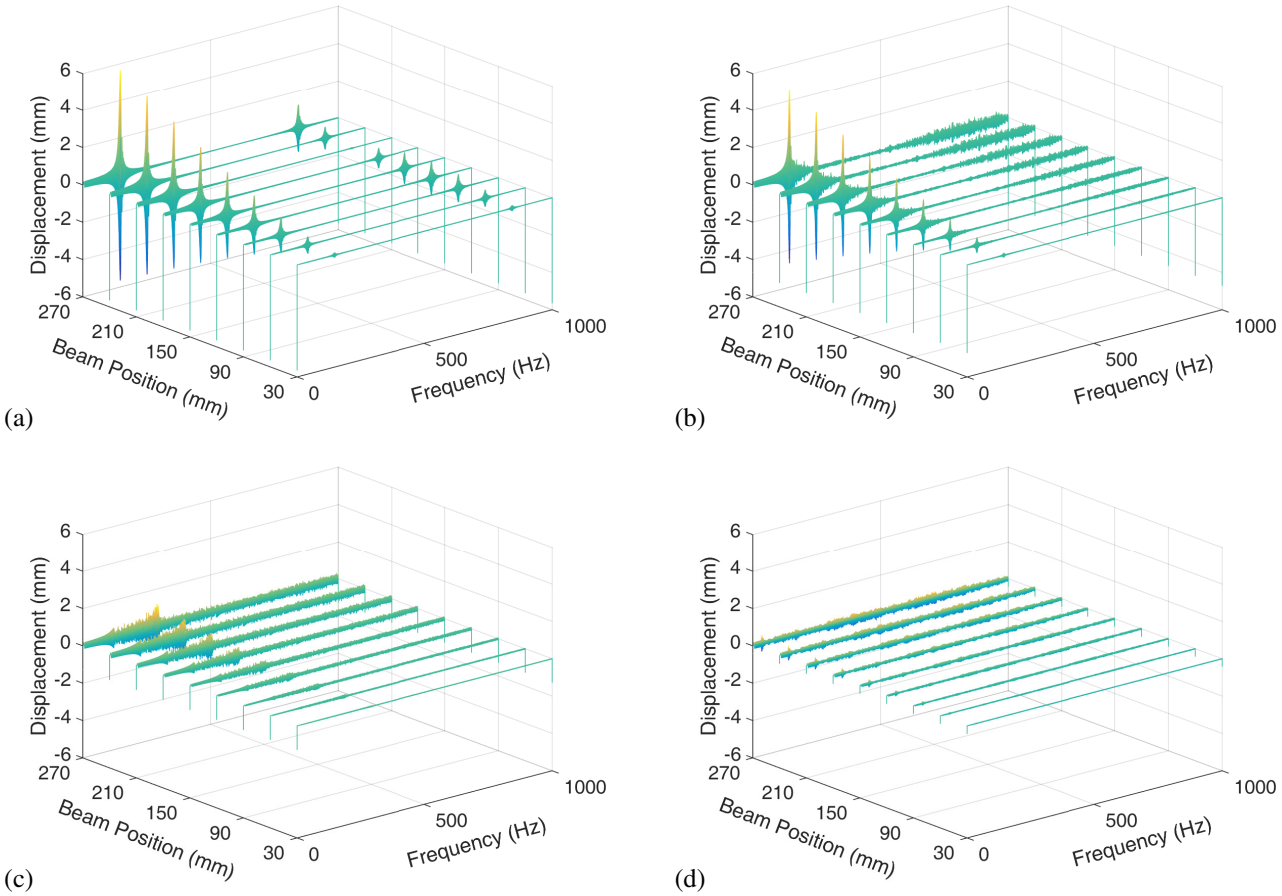

Figure 6. Frequecy response of the the cantilever beam at the rotating speed of 3000 rpm: (a) no spheres, (b) 10 spheres (50 mm hole), (c) 20 spheres (100 mm hole), (d) 40 spheres (200 mm hole).

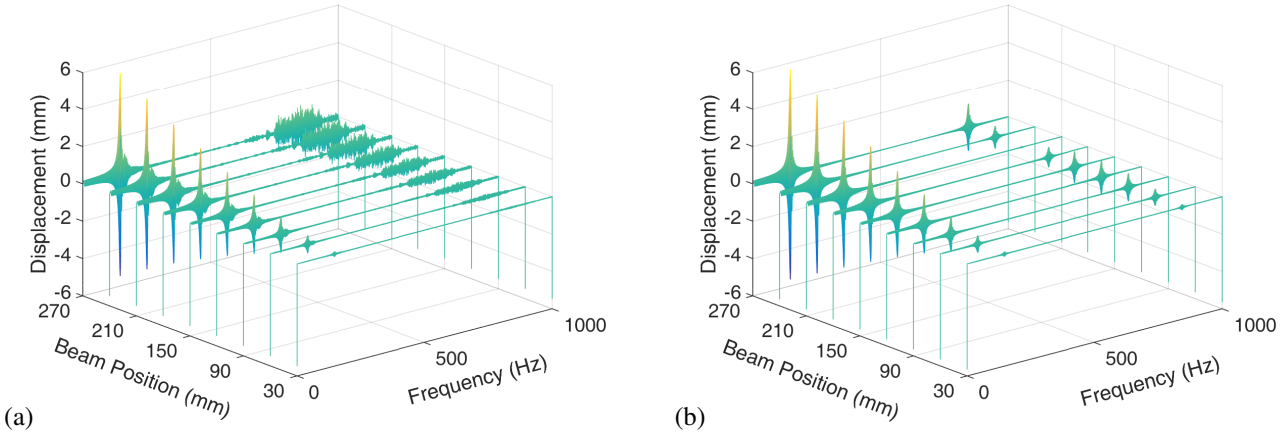

Figure 7. Frequency response of the cantilever beam (10 spheres, 3000 rpm): (a) $s = 0.3$ mm, (b) $s = 0.5$ mm.

In general, the bigger the gap is, the bigger the vibration amplitudes of the beam must be for an appropriated performance of the damper;

- the length of the damper plays an important role in the attenuation of the resonance peaks, and different effects may occur for different lengths of the damper. Such characteristics is related to vibration amplitudes of the beam as it vibrates in different mode shapes;

- the rotating speed does not significantly change the obtained results.

5. ACKNOWLEDGEMENTS

The authors acknowledge the support given to this project by FAPESP (Fundação de Amparo à Pesquisa do Estado de São Paulo), CNPq (Conselho Nacional de Desenvolvimento Científico e Tecnológico), grant no. 301118/2018-3, and USP (Universidade de São Paulo), PUB scholarship no. 1444.

6. REFERENCES

Cui, Z., Wu, J.H., Chen, H. and Li, D., 2011. "A quantitative analysis on the energy dissipation mechanism of the non-obstructive particle damping technology". *Journal of Sou*, Vol. 330, pp. 2449–2456.

Koch, S., Duvigneau, F., Orszulik, R., Gabbert, U. and Woschke, E., 2017. "Partial filling of a honeycomb structure by grannular materials for vibration and noise reduction". *Journal of Sound and Vibration*, Vol. 393, pp. 30–40.

Kubiak, J., Urquiza, G., Rodriguez, J.A., Gonzalez, G., Rosales, I., Castillo, G. and Nebradt, J., 2009. "Failure analysis of the 150 mw gas turbines blades". *Engineering Failure Analysis*, Vol. 16, pp. 1794–1804.

Lourenço, N.J., Graça, M.L.A., Franco, L.A.L. and Silva, O.M.M., 2008. "Fatigue failure of a compressor blade". *Eng*, Vol. 15, pp. 1150–1154.

Lu, Z., Wang, Z., Zhou, Y. and Lu, X., 2018. "Nonlinear dissipative devices in structural vibration control: a review". *Journal of Sound and Vibration*, Vol. 423, pp. 18–49.

Nicoletti, R. and Liebich, R., 2018. "Analysis of long wind turbine blades with shape memory alloy wires in super-elastic phase". *Journal of Intelligent Material Systems and Structures*, Vol. 29, No. 15, pp. 3108–3123.

Thomson, W.T. and Dahleh, M.D., 1998. *Theory of vibration with applications*. Prentice Hall, Upper Saddle River.

Xu, Z., Wang, M.Y. and Chen, T., 2004. "An experimental study of particle damping for beams and plates". *Journal of Vibration and Acoustics*, Vol. 126, pp. 141–148.

Xu, Z., Wang, M.Y. and Chen, T., 2005. "Particle damping for passive vibration suppression: numerical modelling and experimental investigation". *Journal of Sound and Vibration*, Vol. 279, pp. 1097–1120.

Yu, Z. and Xu, X., 2009. "Failure investigation on failed inducer blades used in locomotive turbocharger". *Engineering Failure Analysis*, Vol. 16, pp. 402–408.

7. APPENDIX

The finite element matrices used in the model of the rotating beam are:

$$\mathbf{M}_e = \begin{bmatrix} \mathbf{M}_u & \mathbf{0} \\ \mathbf{0} & \mathbf{M}_v \end{bmatrix}; \quad \mathbf{G}_e = \begin{bmatrix} \mathbf{0} & -\mathbf{G}_{uv} \\ \mathbf{G}_{uv}^T & \mathbf{0} \end{bmatrix}; \quad \mathbf{K}_e = \begin{bmatrix} \mathbf{K}_u & \mathbf{0} \\ \mathbf{0} & \mathbf{K}_v \end{bmatrix}; \quad \mathbf{K}_{\Omega e} = \begin{bmatrix} \mathbf{K}_{\Omega u} & \mathbf{0} \\ \mathbf{0} & \mathbf{K}_{\Omega v} \end{bmatrix} \tag{6}$$

$$\mathbf{f}_e = \begin{Bmatrix} \mathbf{f}_u & \mathbf{0} \end{Bmatrix}; \quad \mathbf{q}_e = \begin{Bmatrix} u_1 & \theta_{u1} & u_2 & \theta_{u2} & v_1 & \theta_{v1} & v_2 & \theta_{v2} \end{Bmatrix}^T \tag{7}$$

where:

$$\begin{aligned} \mathbf{M}_u &= \rho A L\, \mathbf{M}_t \\ \mathbf{M}_v &= \rho A L\, \mathbf{M}_t + \frac{\rho I}{L}\, \mathbf{M}_r \\ \mathbf{G}_{uv} &= 2\Omega \rho A L\, \mathbf{M}_t + \Omega \frac{\rho I}{L}\, \mathbf{M}_r \\ \mathbf{K}_u &= \frac{EA}{L}\, \mathbf{M}_r \\ \mathbf{K}_v &= \frac{EI}{L^3}\, \mathbf{K} \\ \mathbf{K}_{\Omega u} &= \Omega^2 \rho A L\, \mathbf{M}_t + \Omega^2 \frac{\rho I}{L}\, \mathbf{M}_r \\ \mathbf{K}_{\Omega v} &= \Omega^2 \rho A L\, \mathbf{M}_t \\ \mathbf{f}_u &= \mathbf{K}_{\Omega u}\, \mathbf{r} \end{aligned} \tag{8}$$

$$\mathbf{M}_t = \frac{1}{420} \begin{bmatrix} 156 & 22L & 54 & -13L \\ & 4L^2 & 13L & -3L^2 \\ & & 156 & -22L \\ sym. & & & 4L^2 \end{bmatrix}; \qquad \mathbf{M}_r = \frac{1}{30} \begin{bmatrix} 36 & 3L & -36 & 3L \\ & 4L^2 & -3L & -L^2 \\ & & 36 & -3L \\ sym. & & & 4L^2 \end{bmatrix} \tag{9}$$

$$\mathbf{K} = \begin{bmatrix} 12 & 6L & -12 & 6L \\ & 4L^2 & -6L & 2L^2 \\ & & 12 & -6L \\ sym. & & & 4L^2 \end{bmatrix} \tag{10}$$

and ρ is the material density, E is the material Young modulus, A is the beam cross section area, I is the cross section second moment of inertia, L is the element length, Ω is the rotating speed, and $\mathbf{r}$ is a vector of the distances between the nodes and the center of rotation.

8. RESPONSIBILITY NOTICE

The authors are the only responsible for the printed material included in this paper.